Bao *et al.*
Journal of Engineering and Applied Science (2022) 69:111
https://doi.org/10.1186/s44147-022-00157-6

Journal of Engineering and Applied Science

RESEARCH Open Access

Study on mechanism and influential factors of progressive collapse resistance of base-isolated structure

Chao Bao[1,2*], Yuhang Zhang[1*], Dahai Lv[1], Huxiang Wang[1], Xiaotong Ma[3], Jixing Cao[4] and Kar Sing Lim[5]

*Correspondence: baochao@nxu.edu.cn; nxu-zyh@foxmail.com

[1] School of Civil and Hydraulic Engineering, Ningxia University, Yinchuan, China
[2] Institute of Earthquake Protection and Disaster Mitigation, Lanzhou University of Technology, Lanzhou, China
[3] School of Civil Engineering, North Minzu University, Yinchuan, China
[4] Department of Civil and Environmental Engineering, National University of Singapore, Singapore, Singapore
[5] Department of Civil Engineering, College of Engineering, Universiti Malaysia Pahang, Kuantan, Malaysia

Abstract

The progressive collapse of the structure caused by the partial failure of the structure will cause severe consequences and massive losses, and structural progressive collapse resistance has always been a hot topic of current research. In order to study the progressive collapse mechanism of base-isolated structures, the test study and numerical simulation of the base-isolated structures were carried out based on the vertical Pushover method and analysis of the variation rule of the capacity of the remaining structure and influence mechanism. The isolation bearing failure position, the size of the beam of the seismic isolation layer, the type of the isolation bearing, and the horizontal stiffness of the seismic isolation layer on the capacity of the remaining structure were compared and analyzed. The results show that the non-uniformity of the beams and the concentrated loading at the nodes were easy to form a linear catenary mechanism, resulting in more severe beam end damage than mid-span damage. In the case of side isolation bearing failure, due to the lack of sufficient lateral restraint, the capacity was significantly lower than other conditions, which were more likely to cause partly collapse. Therefore, setting more transfer paths to improve the structure's resistance to progressive collapses was necessary. Increasing the size of the beam of the seismic isolation layer could improve the capacity of the remaining structure of the alternate load path in the base-isolated structure. The changes in the horizontal stiffness of the seismic isolation layer and the type of the isolation bearing have little effect on the progressive collapse resistance capacity of the remaining structure.

Keywords: Base-isolated structure, Pushdown analysis, Model test, Progressive collapse, Remaining structure

Introduction

Progressive collapse means that under the action of accidental loads such as terrorist attacks, fires, and vehicle impacts, the local damage to the structure causes a chain reaction and then causes damage to other parts of the structure, resulting in the collapse of

the overall structure. Structural collapse accidents cause heavy casualties and property losses, so the progressive collapse of structures [1–3] has always been a hot issue in current research.[1]

The progressive collapse analysis of the reinforced concrete (RC) structure was based mainly on a threat-independent alternative path. Local failure that may lead to the progressive collapse of the structure was simulated by removing critical load-bearing members [4–7]. Existing studies on the progressive collapse of the RC frame structure mainly focus on theoretical analysis, experimental studies, and numerical simulation of substructures [8–13]. In terms of theoretical research. Amiri et al. [14] considered the effect of the existing structural capacity on the DIF value of the RC structure. Jiang et al. [15] proposed an improved configurational fragility theory, which considered the joints from the rigid transition connection to the hinge. Azim et al. [16] analyzed the factors affecting the progressive collapse resistance of the RC frame structure and compiled and presented the experimental collapse results. According to Feng [17] based on the redundancy assessment of aging reliability in corroded RC, the frame structure was quantitatively analyzed. In terms of experimental research and numerical simulation, Lu et al. [18] and Yu et al. [19] explored column removal tests on the reinforced concrete beam-slab substructure model and found that the beam-slab structure resisted the beam-slab arching mechanism and bending mechanism in small deformations, while resisted collapse through beam-slab catenary effect and tensile film effect on large deformation. Ma et al. [20] designed the column demolition test of the 1/3 scale reinforced concrete slab column structure, and the model showed punching shear failure mode and resisted progressive collapse through the tensile film effect of the slab. Qian et al. [21] numerically studied the behavior of post-tensioned PC structures against progressive collapse. Deng et al. [22] conducted 6 tests on the RC frame with high strength concrete strength and found that using high-strength concrete could further improve the compression arch effect, reducing the catenary affect capacity. Wang et al. [23] designed four beam-column substructures and found that the beam-slab effect cannot be ignored. Liu et al. [24] discussed an experimental and numerical study on the progressive collapse of a prefabricated reinforced concrete frame. They found that the collapse resistance contribution rate of the prefabricated monolithic specimen was lower than that of the cast-in-place comparison specimen.

Compared to the traditional seismic structure, the base-isolated structure could significantly reduce the seismic response of the building by setting the seismic isolation bearing on the foundation to form a seismic isolation layer, prolonging the structure period. At the same time, because the seismic isolation layer had a weak restraint capacity on the superstructure, it was inevitable to cause a significant difference from the traditional

seismic buildings. It was necessary to conduct relevant research on the progressive collapse of the base-isolated structure under accidental loads. Tavakoli et al. [25] conducted a nonlinear static analysis on the base-isolated structure to analyze the structure's progressive collapse resistance collapse ability. It was found that the isolation system did not play an influential role in improving the structure's collapse resistance but did not enhance the anti-collapse ability of the base-isolated structure. Huang et al. [26] based on the introduction of a seismic damage model of isolators, a reliability analysis of base-isolated frame-wall structures was conducted using the global reliability method and the performance of progressive collapse resistance and structural seismic damage can be acquired. Yang et al. [27] study the progressive collapse performance of the base-isolated frames supported by stepped foundation in mountainous areas under two-directional coupled dynamic excitation and advised the design of progressive collapse of the frame structure of the base-isolated frames supported by stepped foundation in mountainous areas. The mechanism and influencing factors of progressive collapse resistance have not been studied. This paper used the base-isolated structure's nonlinear static Pushdown analysis method to conduct the test research and the finite element analysis verification of its capacity and the collapse mechanism. The influence of the isolation bearing failure position, the size of the beam of seismic isolation layer, the type of isolation bearing, and the isolation bearing stiffness on the collapse mechanism of the base-isolated structure were compared and analyzed.

Methods

Pushdown analysis methods for base-isolated structure

Pushdown analysis used the pushover analysis method to analyze the progressive vertical collapse of structures. Pushover analysis, namely the nonlinear static analysis method, was a method to evaluate existing structures and design new structures based on performance, mainly used to evaluate the seismic performance of structures. Pushover analysis focuses mainly on the lateral collapse of structures, while pushdown analysis focuses on the vertical collapse of structures. In pushdown analysis, there were two vertical loading modes: full-span and damaged loading, mainly divided into force loading and displacement loading. The full-span load refers to the vertical load of the structure, which increases uniformly in each span. In the failure span loading, only the increase of the failure span caused by the failure beam element was considered, while the vertical load of other unaffected spans remains unchanged. This paper adopted the Pushdown analysis method of damaging cross-loading proposed by Khandelwal et al. [28] for analysis. Increasing loads were applied to the initial buckling region, and gravity loads were applied to the entire region. Pushdown analysis based on displacement control was used, as depicted in Fig. 1.

Testing model design

In this study, a student dormitory building is used as a prototype for the experimental model design. The project is a reinforced concrete frame structure with a total of 6 floors. The height of each floor is 3.30m, and the total height is 19.30m. Category C building, seismic fortification intensity of 8°, basic seismic acceleration 0.3g, design earthquake group 2, and site characteristic period 0.4s. The testing model

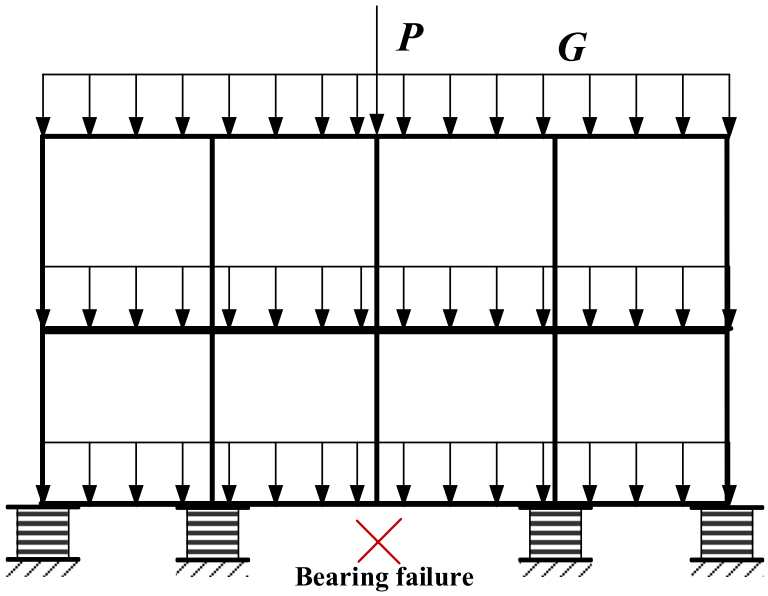

Fig. 1 Pushdown analysis

Table 1 Parameters of isolation bearing

Project	Parameters	Project	Parameters
Product outer diameter (mm)	100	Height (mm)	53
The thickness of the protective layer (mm)	5	First shape factor S1	15.0
Rubber outer diameter (mm)	90	Second shape factor S2	5.0
Lead diameter (mm)	15	Reference surface pressure	10
The thickness of each layer of rubber (mm)	1.5	Vertical stiffness (kN/mm)	152.3
Number of rubber layers	12	Yield force (kN)	1.409
The thickness of each layer of steel plate (mm)	1	Stiffness after yielding 100%	0.139
Number of layers of thin steel plate	11	Equivalent stiffness 100% (kN/mm)	0.217
The thickness of the sealing plate (mm)	12	Equivalent damping ratio 100%	21.9

was composed of isolation bearings and a superstructure model. The superstructure adopted the RC frame structure. The primary reference parameters of the frame testing model of the base-isolated structure were as follows: the section size of the frame column was 150mm×150mm, the size of the upper frame beam was 100mm×150mm, and the size of the beam of the seismic isolation layer was 100mm×200mm. Moreover, the isolation bearing was selected with a diameter D 100mm lead rubber bearing (LRB). The specific parameters of isolation bearing were demonstrated in Table 1, and the size of the testing model is depicted in Fig. 2. By Chinese code [29], the compressive strength of concrete at the age of 28 days was determined by averaging the tested values of three 150 mm×150mm×300mm were 25.6 MPa. The yield strength of reinforcing f_y and the ultimate strength of reinforcement f_t was determined by averaging the tested values of three 400-mm long bars from the same batch of bars used in the test. The yield strength of reinforcement f_y was 238MPa, and the ultimate strength f_t was 319MPa.

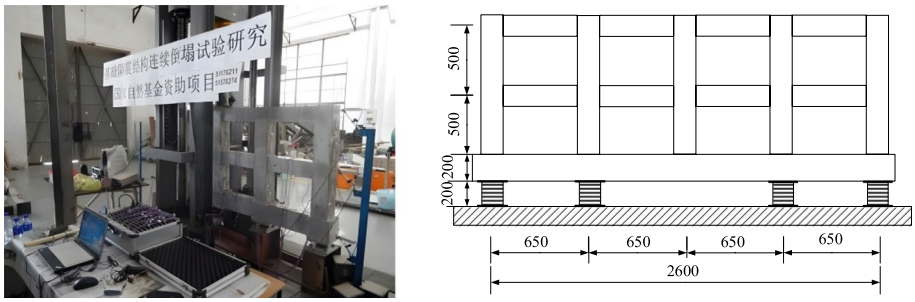

(a)Testing model (b)Model size

Fig. 2 Size of testing model. a Testing model. b Model size

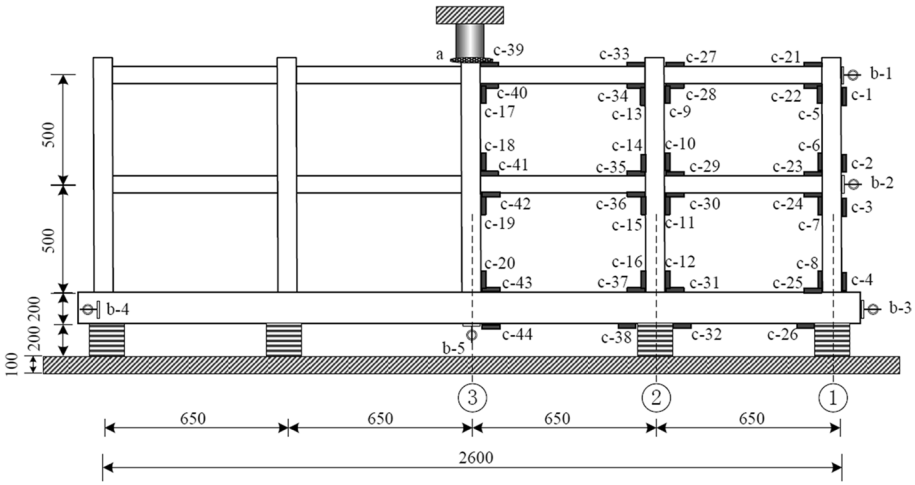

Fig. 3 Sensor layout and number

The layout of measuring points was one of the critical points of the model test. According to the model and test characteristics, as well as the actual demand for data and test equipment limitations, the response information of the whole and local components was mainly measured. According to the overall measurement and local measurement, the test device was designed and tested to study the progressive collapse behaviors and anti-progressive collapse performance of the remaining structure after the initial failure of the base-isolated structure.

Force and vertical displacement sensors were set at the initial failure position of the bearing. Horizontal displacement sensors and steel bar strain sensors were arranged at both ends of the beam of the isolation layer in the initial failure isolation bearing section, and the deformation and crack development of the superstructure, and the deformation of the remaining bearing were observed and recorded in the whole process of the test. The specific layout and number of the sensors are shown in Fig. 3, in which a, b, and c represent the force, displacement, and strain sensors, respectively. The displacement sensor was used to monitor the displacement response during the test, and the force sensor was used to monitor the internal force redistribution process of the damaged structure.

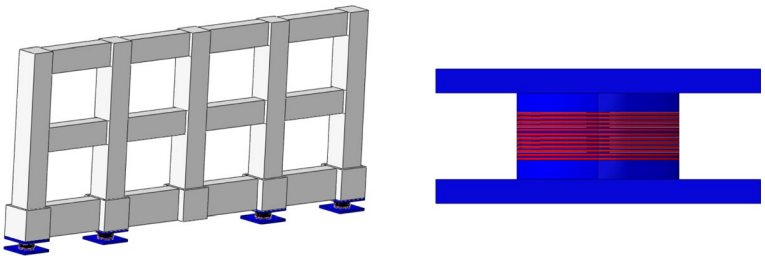

(a) Base-isolation structure (b) Isolation bearing

Fig. 4 Simulation model. a Base-isolation structure. b Isolation bearing

The finite element software ABAQUS established the finite element model of the base-isolated structure. The perspective and plan view of the structure is presented in Fig. 4. The beams, slabs, and columns used the hexahedral reduced solid element C3D8R, and the steel reinforcement used the three-dimensional two-node truss element T3D2, and the steel skeleton was embedded in the concrete through the EMBED command. The isolation bearing was modeled with solid elements. Due to the incompressible or almost incompressible properties of the material, the 8-node hexahedral hybrid reduction element C3D8RH was required for the material. The hybrid formula allowed the nodal displacement of the element to be used only to calculate the deviatoric strain and deviatoric stress, and the compressive stress of the element was determined by an additional degree of freedom, which could prevent the problem of volume self-locking. The reduced integration could reduce the integration points and increase the calculation efficiency. The lead core was a conventional material. In order to prevent the self-locking problem of shear force, it was recommended to use the reduced integration 8-node linear hexahedron element C3D8R for calculation. Due to the small deformation, the steel could use the 8-node hexahedral incompatible element C3D8I to prevent the shearing cut self-locking problem. The superstructure was connected to the isolation bearing by a Tie connection. The mesh size of the finite element model is determined according to the experimental model mesh division suggestions. The concrete mesh size is 50mm, the reinforcement mesh size is 60mm, and the steel plate and rubber mesh size in the isolation bearing are the same, which is 50mm. The lead core grid size is 30mm, and the grid sensitivity analysis is carried out. The impact of the grid on the results is acceptable.

Because the concrete was cast-in-place, the merge command was used in the numerical model to perform Boolean operations on the concrete elements to form a whole. Reinforcement was embedded into the concrete using the EMBED command without considering the bond slip between reinforced concrete. The mesh sizes of reinforcement and concrete elements were adjusted according to the model by trial calculation. The constraints in the direction of U1 and U2 were set on the failure column, and the failure column only shifted up and down the direction of U3 in the loading process. The model adopts the fixed constraint mode at the bottom of the column instead of the ground anchor action in the test. In the numerical simulation, displacement control was used to load the structure, and coupling reference points were set on the failure cylinders to ensure the convergence of the model.

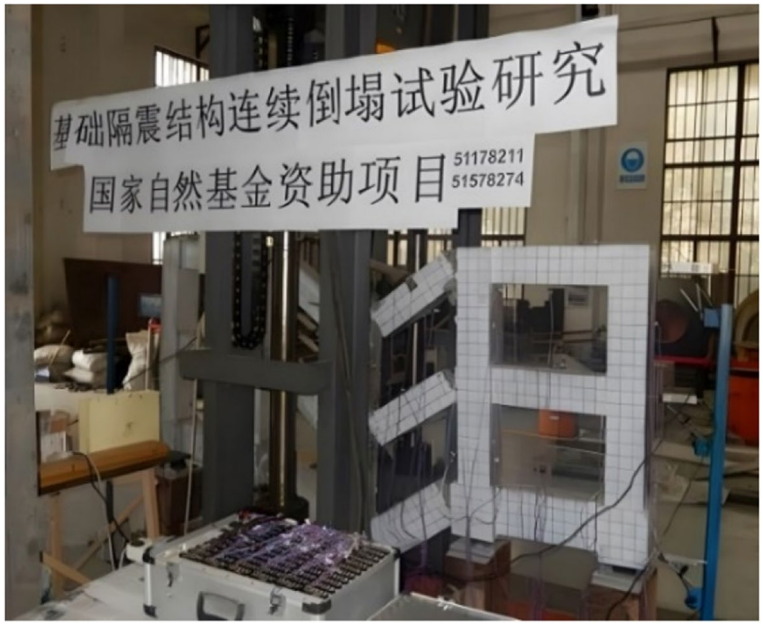

Fig. 5 Testing model

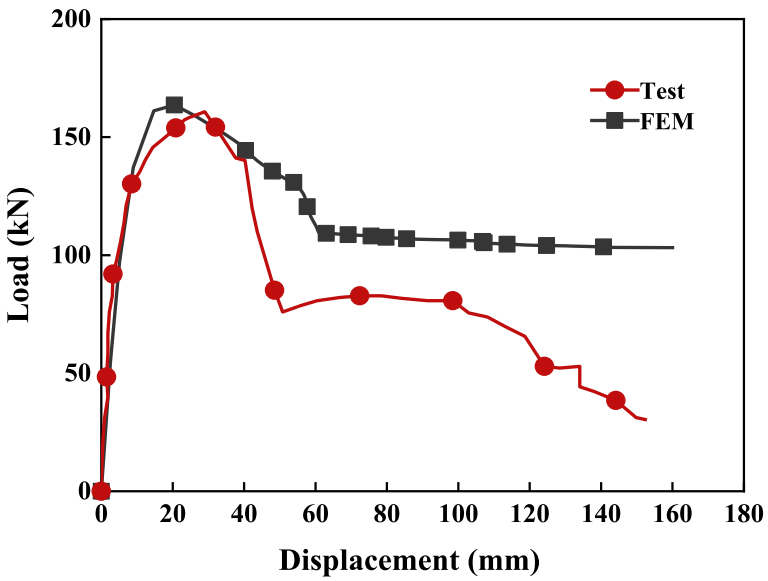

Fig. 6 Comparisons of test and FEM results

Results and discussion

Overall collapse and failure mode

To verify the rationality and reliability of the selected structural elements and the finite element parameters in the finite element model, test analysis and ABAQUS finite element model simulation analysis of a single frame were carried out, respectively. The testing model is shown in Fig. 5.

From the vertical pushover diagram of test and simulation in Fig. 6, it could be observed that during the whole collapse process, from the beginning of loading to the

(a) Test

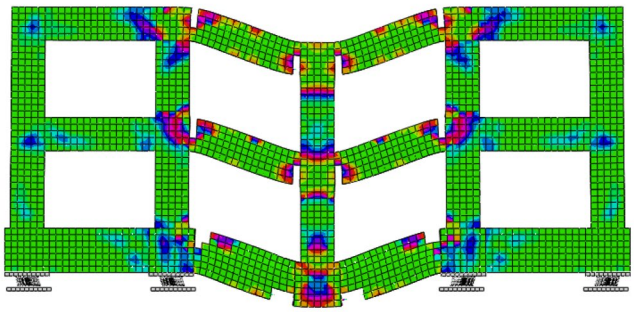

(b) FEM

Fig. 7 Comparisons of failure modes between test and FEM results

complete failure of the structure, both the testing model and the finite element model went through the ascending section to reach the same ultimate capacity. The concrete cracked, the capacity of the remaining structure decreased sharply to a specific value and then went through the transition stage, and finally, the reinforcement fracture structure failed. With the gradual improvement of structural nonlinearity, due to the difference between the testing model and finite element model in constitutive and boundary constraints, static loading reinforcement bar stress remains unchanged until the reinforcement stage and the difference between the two rises. With the increasing vertical displacement of the failed column, the stiffness of the frame structure was further decreased.

By comparing the testing structure and the simulated tensile damage condition in Fig. 7, the deformation of the adjacent span beam-column members was observed, and apparent cracks appeared in the members. However, the in-plane tilt phenomenon appeared in the adjacent span at the end of loading, indicating that the seismic isolation and the timely release of the reaction force from the layer could play a specific protective role on the adjacent span internal members, but there was a risk of causing the remaining structure to tilt or even overturn. From the failure mode of the whole testing model, the final failure of the structure was more similar to the "brittle failure" mode of the less reinforced beam. The main reason for this failure

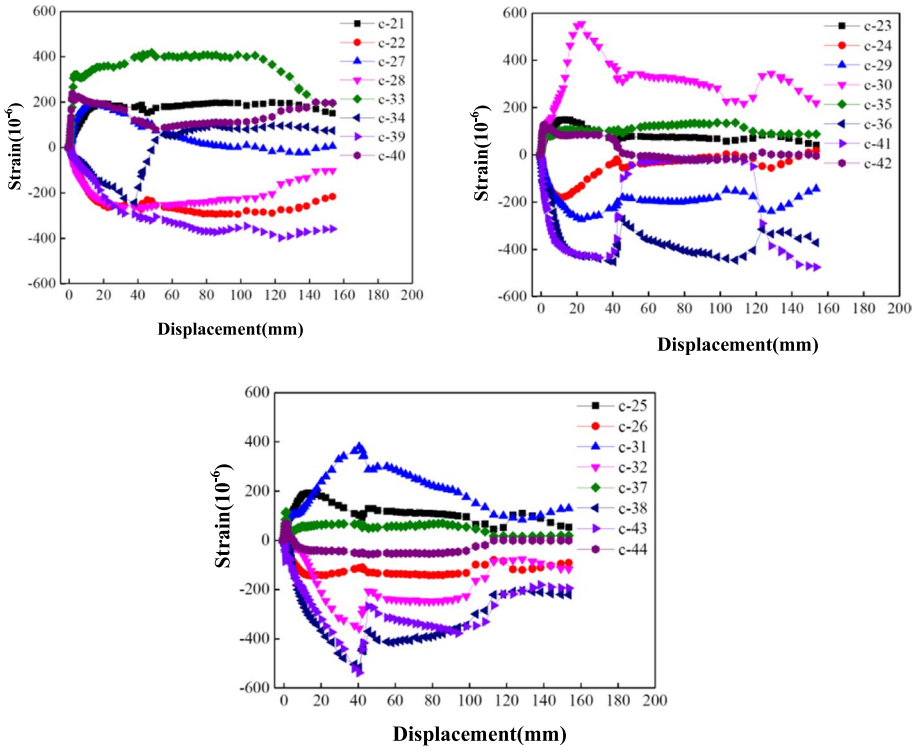

Fig. 8 Surface strain of concrete at beam end

mode was that the concentrated loading at the joint was easy to form a linear catenary mechanism, resulting in more severe damage at the beam end than at the middle of the beam span. The beam end would be damaged when the load increased to a certain extent.

Remaining structural strain

The strain curve of the concrete surface at the end of the beam could be seen in Fig. 8 that individual strain data are discrete. The main reason was that the location of concrete cracks was uncertain. However, the strain curve of concrete at the end of the beam generally was confirmed to the law of concrete strain variation and can reflect the internal force at the end of the member. The change of surface strain of concrete was also related to the response of the remaining structure. Various strain curves in Fig. 8 shows a sudden change of strain values in different degrees in the range of vertical displacement from 29.50 to 45.50mm. Combining with the relationship curve in Fig. 6, it could be found that the structure has completed the transformation from beam mechanism to catenary mechanism in this vertical displacement range. During this process, the sudden release of external loads and the sudden decrease of internal forces caused a significant change of strain at the end of the beam.

Displacement and damage of the isolation bearing

The displacement condition of the isolation bearing in the test and simulation was extracted and tested. Figure 9 was a comparison diagram of the displacement derived

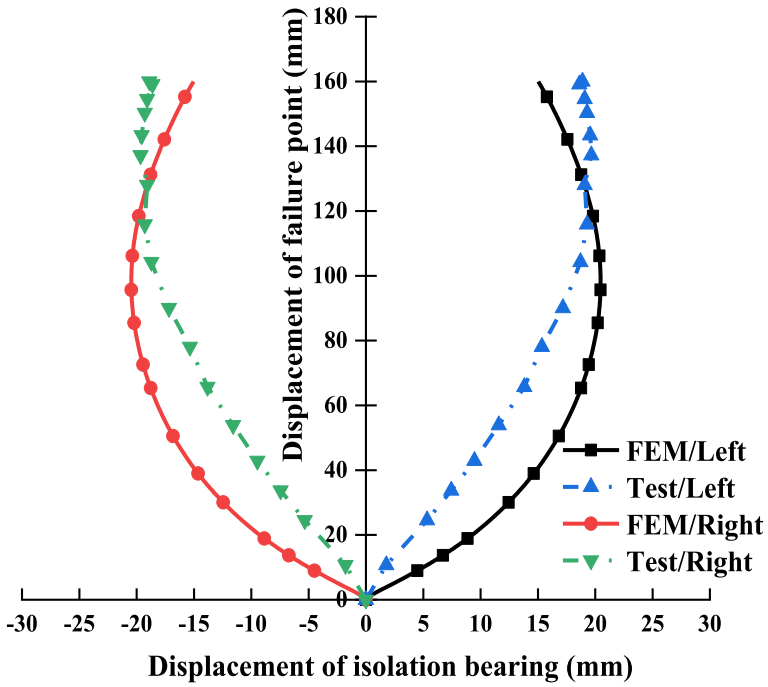

Fig. 9 Displacement of isolation bearing comparison

(a) Left (b) Right

Fig. 10 Test deformation diagram of the bearing

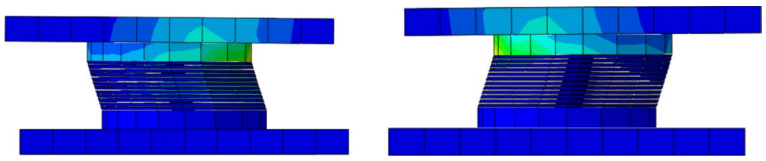

(a)Left (b)Right

Fig. 11 Simulation deformation diagram of bearing

from the isolation bearing tested and the finite element analysis. Figures 10 and 11 were the isolation bearing test and finite element analysis deformation diagram.

It was found that the stiffness of the upper structure was much greater than that of isolation bearings. The relative displacement between the isolation bearings was minimal and could be ignored. The isolation bearings on both sides of the failed isolation bearings were extracted for comparison. The changing trend of the isolation bearing

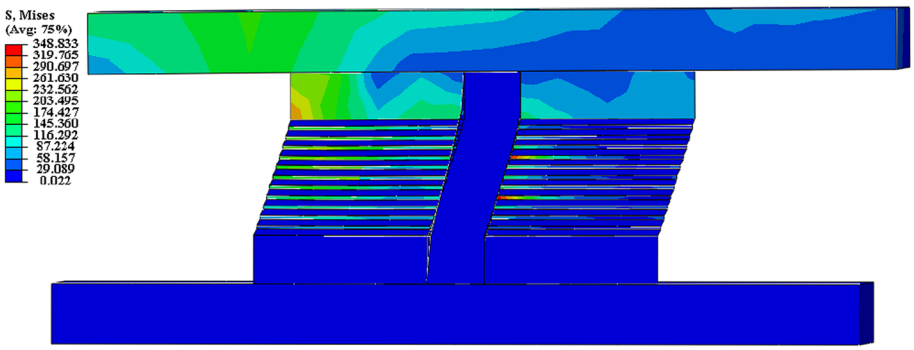

Fig. 12 Internal failure diagram of the bearing

displacement was the same, the maximum displacement of the isolation bearing was similar, and the difference was only 3mm. The simulated isolation bearings had the same shape and size, solid elements simulated the isolation bearing, and the constitutive adopted the constitutive relationship obtained from the experiment. So, the use of solid elements to simulate isolation bearings had good applicability, as shown in Fig. 11. It can be seen from the results of the finite element model and the experimental model that the finite element model could well reflect the progressive collapse of isolation bearing capacity and collapse mechanism of the base-isolated structure and could reveal the mechanism of progressive collapse. Therefore, the finite element model had particular applicability and accuracy.

The failure condition of the adjacent isolation bearings under the failure condition of the center column isolation bearing was extracted in Fig. 12, and the internal failure condition of the lead core isolation bearing was analyzed. It could be seen from the simulation process that as the vertical displacement of the center column increased, the isolation bearing was affected by the horizontal thrust of the beam of the seismic isolation layer, and the local stress of the isolation bearing became larger and larger, and the stress on the left and right half of the isolation bearing was differentiated. The stress at the end near the failed isolation bearing increases gradually. The stress at the end away from the failed isolation bearing with little change, the lead-core isolation bearing under uneven compression, with the increase of horizontal displacement, the stress on both sides of the adjacent isolation bearing of the failed isolation bearing would aggravate the non-uniformity of the compressive stress distribution.

Node damage

When the test was completed, most of the concrete near the beam-column joint area was crushed, and the structural damage mainly occurred at the beam end and the beam-column joint areas were demonstrated in Fig. 13. With the increase of displacement, the plastic hinge fails, and the bending moment at the beam end decreases. At this time, the reinforcement is tensioned, the axial force in the beam provides anti-collapse bearing capacity. However, when the components were finally destroyed, the tensile reinforcement was generally constricted and fractured. The concrete in the compression area was crushed and broken. Equivalent plastic strain clouds mapped in the finite element model were extracted. When the maximum principal strain of the element reached ε_{max} =0.01,

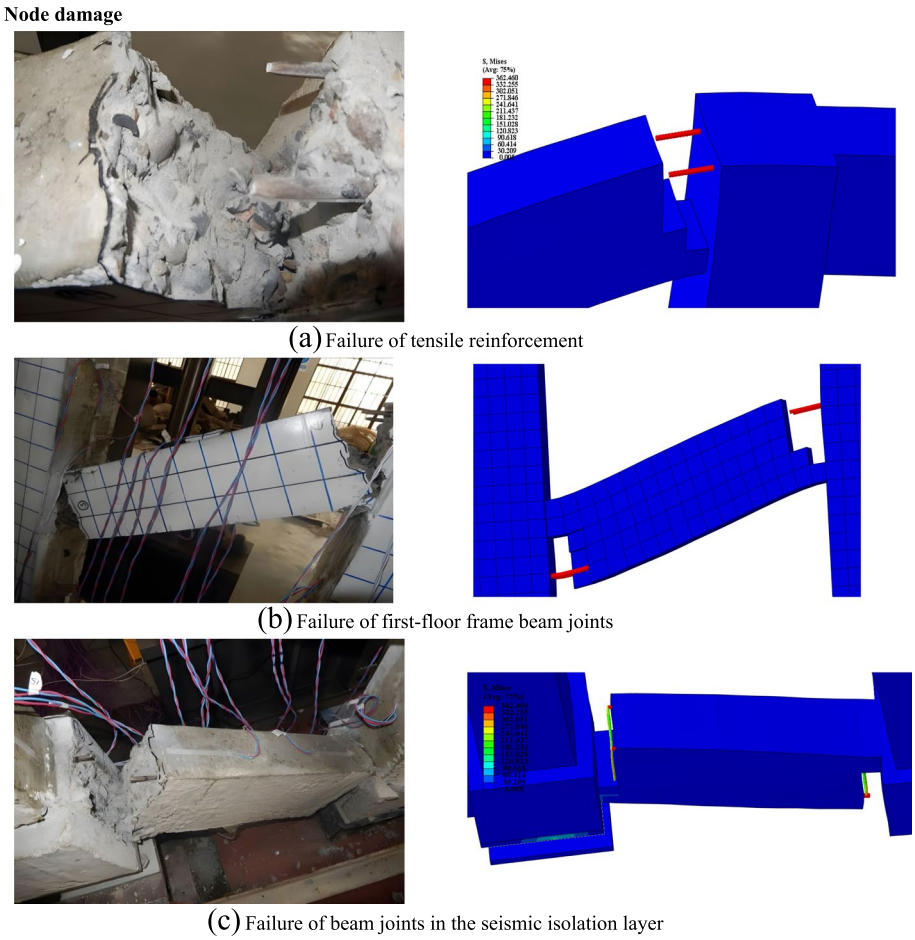

Fig. 13 Failure modes of joint areas. **a** Failure of tensile reinforcement. **b** Failure of first-floor frame beam joints. **c** Failure of beam joints in the seismic isolation layer

the element failed. It could be seen from Fig. 13 that the tensile reinforcement at the beam end was broken. The damage position of the concrete was similar to the test, and the numerical model of a layer of frame beam end concrete crushed, seismic isolation layer on both sides of the beam end damage was severed, a large number of unit failure, node damage similar to test, edge beam under large deformation were apparent torsion damage, caused unit more than the ultimate strain. The failure location of the side beam in the test was consistent with the simulated distribution. The comparison between numerical simulation and test failure shows that numerical simulation could well reflect experimental phenomena.

Analysis of influencing factors of progressive collapse mechanism of base-isolated structure

In order to further study the vertical progressive collapse mechanism and capacity of the base-isolated structure, this paper selects four main factors that affected the progressive collapse mechanism of the base-isolated structure, the failure position, the beam height of the isolation layer, and the stiffness of the isolation layer, and the type of isolation bearing was studied. Through the establishment of 24 finite element models, the

Table 2 Model parameters and numbers

Factors	Model parameters		Working model
	Parameter	Other parameters (failure position)	
Failure position	Middle isolation bearing	-	A1
	Side isolation bearing		A2
	Middle-side isolation bearing		A3
The height of the beam of isolation layer(B×H)	100×200	Middle/side/middle-side	B1-B3
	100×175		B4-B6
	100×150		B7-B9
Type of isolation bearing and isolation layer stiffness (horizontal equivalent stiffness)	Non-isolated	Middle/side/middle-side	C1-C3
	LRB100		C4-C6
	LNR100		C7-C9
	LRB100 Horizontal equivalent stiffness 0.3		C10-C12

pushdown curve of each finite element model and the failure condition process of the components were obtained using the pushdown analysis method. The parameters and numbers of each model are depicted in Table 2.

Failure position analyses

In order to analyze the influence of crucial isolation bearing failure position on the structure's resistance to progressive collapse, the working model numbers A1–A3 in Table 2 were selected for analysis.

Load-displacement curve analysis

Figure 14 shows the load-displacement curve at different failure positions. Remaining structural capacity and displacement at different failure positions were extracted, as demonstrated in Table 3. The data in the table shows that the peak capacity of the remaining structure under the A2 working model was only 97.74kN, which had been significantly reduced, which was only 60% of the failure case of the middle isolation bearing, which was more likely to cause the partial collapse of the structure. The reason for the analysis was that due to the lack of sufficient lateral restraint of the failure position of the side isolation bearing, only the isolation bearing provides lateral restraint on one side, resulting in a decrease in the capacity of the remaining structure and compared with the A3 working model; the beam mechanism displacement was 18 mm; and the A3 working model was 18 mm. There was a delay in reaching the peak value of the beam mechanism, and the peak value between the two was not much different. The peak value of the beam mechanism of the capacity of the remaining structure under the A1 working model was 163.6kN, slightly higher than the A3 working model. The beam mechanism of the capacity of the remaining structure was 157.7kN. After the peak value, the capacity of the remaining structure of the two catenary phases did not increase significantly. The displacement of the adjacent isolation bearings at the failure position of the A1 and A3 working models was minimal, while the displacement of the A2 working model was only

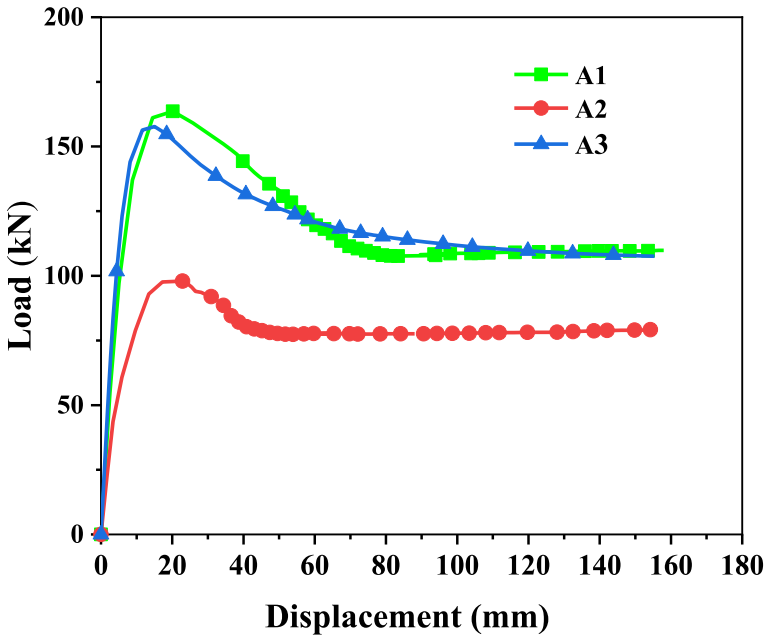

Fig. 14 Load-displacement curves of different failure positions

Table 3 Remaining structural capacity and displacement at different failure positions

Working model	Beam mechanism peak (kN)	Beam mechanism displacement (mm)	Catenary peak (kN)	Catenary displacement (mm)	Bearing displacement	
					U_{min}	U_{max}
A1	163.6	20	109.3	142	−22	22
A2	99.7	23	-	-	-	5
A3	157.7	18	112.4	150	−23	21

5mm, which also shows that the side span was to the collapsed span frame beam. The axial restraint was significant, and the capacity of the remaining structure was also high.

Analysis of component failure condition during the collapse

According to GSA [30] and DoD [31] advice, if the displacement of the failed column reached 1/5 of the single beam span, the member was considered invalid. In this study, the synergistic effect of the beam-slab substructure under large deformation was considered, and the vertical displacement limitation was set at 160mm, which equals 1/4 of the beam span of 650mm. The specification stipulates [35] that the maximum horizontal displacement of the isolation bearing under rare earthquake should not exceed the smaller 0.55 times its effective diameter and three times the total thickness of the layer. In the case of failure of the center column isolation bearing, the compression damage was mainly concentrated on both sides of the failed column, and the horizontal displacement of the side isolation bearing was the largest due to the lack of sufficient lateral restraint of the side isolation bearing. The seismic isolation bearing was subjected to a large horizontal displacement under the horizontal action of the beam. If the horizontal

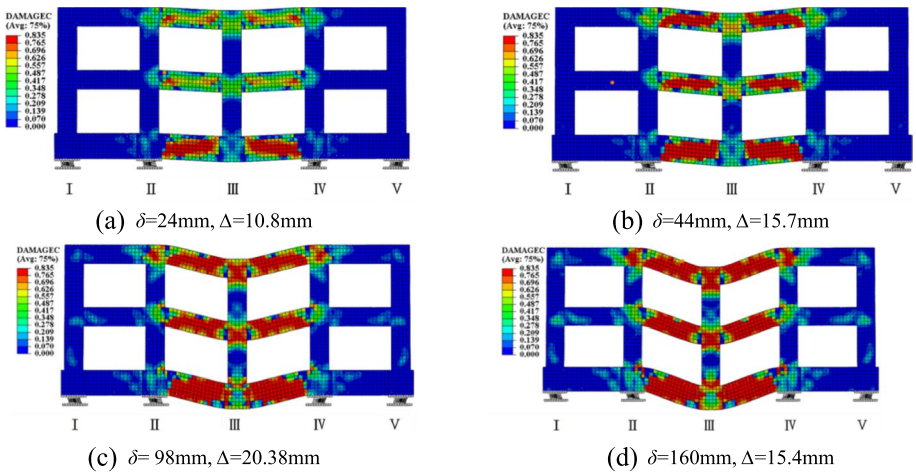

Fig. 15 The failure condition of the middle isolation bearing. **a** δ=24mm, Δ=10.8mm. **b** δ=44mm, Δ=15.7mm. **c** δ= 98mm, Δ=20.38mm. **d** δ=160mm, Δ=15.4mm

displacement limit of the isolation bearing was exceeded, the structure was declared to fail.

The overall failure form of the structure was analyzed based on the failure of the middle isolation bearing. For the convenience of description, the concrete columns were numbered from left to right as I, II, III, IV, and V. As presented in Fig. 15 (a), when the vertical displacement of the top of the failed column δ reached 24mm, the II and IV span beams inclined slightly, and the horizontal displacement of the bearing Δ began to move. The compression failure of column II and column IV beam-column joints in the beam of the seismic isolation layer began (see Fig. 15 b). When δ reached 44mm, the concrete was crushed at both ends of the failed isolation bearing. The tensile reinforcement began to yield, and the isolation bearing displacement was further increased (see Fig. 15 c). When δ reached 98mm, the deformation of beams on both sides of the failed isolation bearing increased, and torsional deformation occurred, and the isolation bearing displacement reached the maximum. When δ reached 160mm, the vertical deformation of the II and IV span was large, the test piece collapsed as a whole, the internal failure force of the member was released, and the displacement of the isolation bearing was reduced. The final failure characteristics of the test are shown in Fig. 15 (d). When the middle column isolation bearing failed, the compression damage was mainly concentrated around the failed column, which was transmitted along the beam span, and the damage to the diaphragm was almost negligible.

When the side isolation bearing failed, the displacement of other isolation bearings changed little, so it would not be discussed. The fault condition of the side isolation bearing was depicted in Fig. 16. When δ reached 30mm, spans I and II inclined slightly, and the beam-column joints on the right side of column II of the seismic isolation layer began to be damaged by compression, as depicted in Fig. 16 (a). When δ reached 93mm, the deformation of spans I and II were obvious, part of the concrete was crushed, and the tensile reinforcement began to yield (see Fig. 16b). When δ reached 120mm, the deformation of spans I and II increased, and the torsional deformation of spans I and II occurred (see Fig. 16c). When δ reached 160mm, the vertical deformation of spans I and

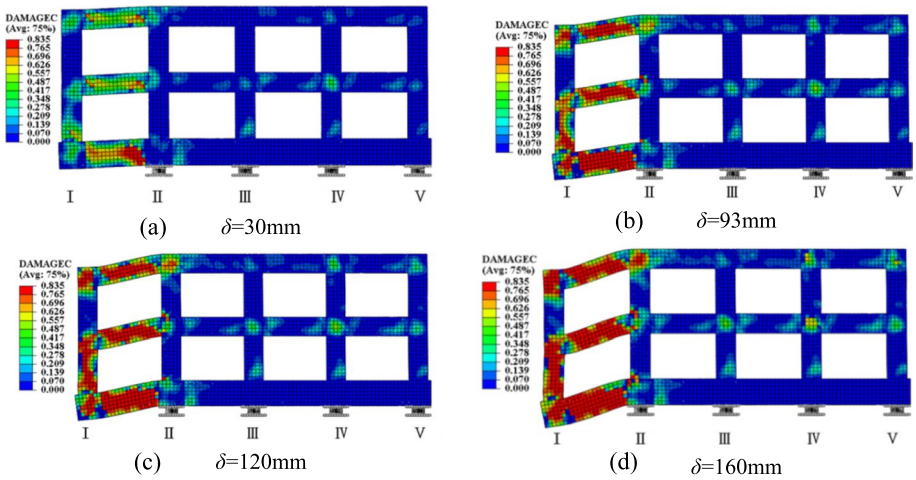

Fig. 16 Failure condition of side isolation bearing. **a** δ=30mm, δ=120mm. **b** δ=93mm, δ=160mm

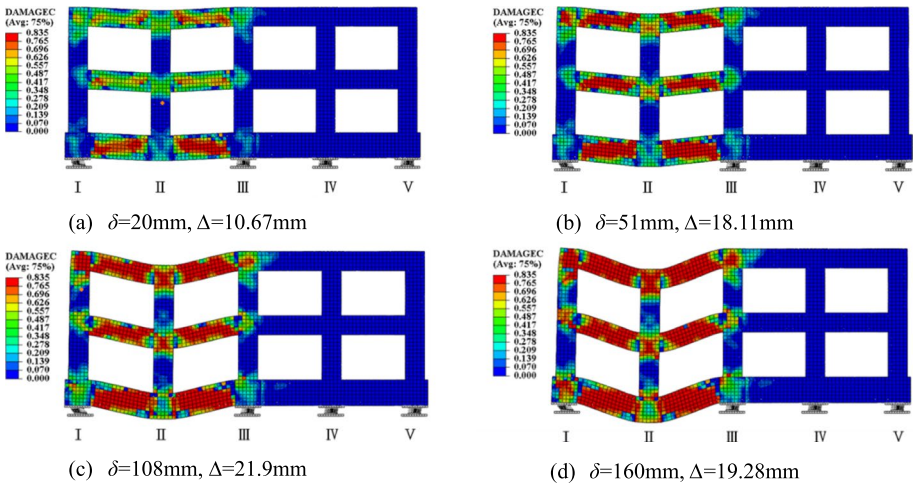

Fig. 17 Failure condition of the middle-side isolation bearing. **a** δ=20mm, Δ=10.67mm. **b** δ=51mm, Δ=18.11mm. **c** δ=108mm, Δ=21.9mm. **d** δ=160mm, Δ=19.28mm

II were large. The specimen collapsed as a whole, and the final failure characteristics of the test are shown in Fig. 16 (d).

When the damage of the mid-span isolation bearing was similar to that of the mid-span isolation bearing was observed in Fig. 17 (a), when δ 24mm, Iand III span beams were slightly inclined, and the displacement of the isolation bearing began to rise. The beam-column joints of column II in the isolation layer began to be damaged by compression, as shown in Fig. 17 (b). When δ reached 51mm, at both ends of the isolation bearing, the concrete was crushed, the tensile steel began to yield, and the displacement of the isolation bearing further increased, as shown in in Fig. 17 (c). When δ reached 108mm, the deformation of the beams on both sides of the failed isolation bearing increased, torsional deformation occurred. The isolation bearing displacement reached a maximum. When δ 160mm, the vertical deformation of I and III spans were large; eventually, the whole collapsed.

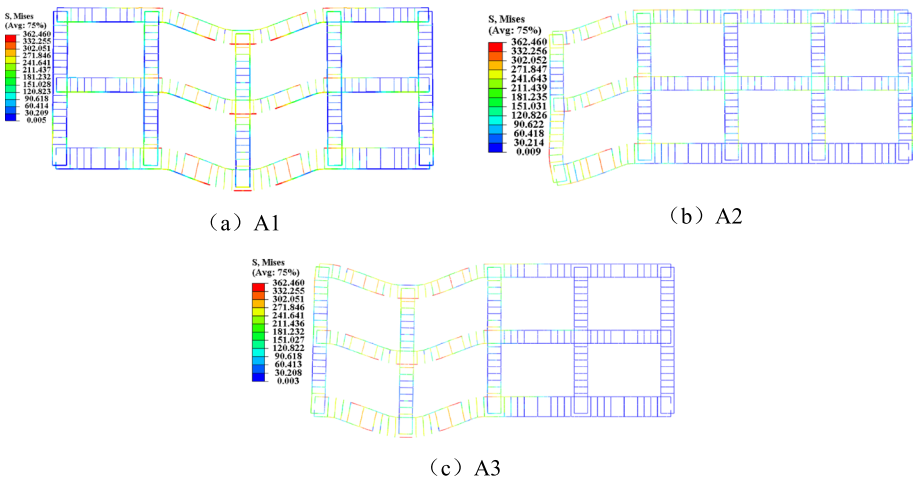

Fig. 18 Mises stress cloud diagram of steel bars in the frame**. a** A1, **b** A2, and **c** A3

Stress condition analysis of bars

When the isolation bearing failed, the internal force of the superstructure would be redistributed due to the change in position of the bottom isolation bearing. In the post-processing, the concrete in the frame was hidden, only the complete skeleton of the steel bar was displayed, and the stress condition of the steel bar in the remaining structure after the failure of the isolation bearing was analyzed. When the equivalent plastic strain of the reinforcement reached 0.1, the reinforcement element failed. Figure 18 shows the Mises stress cloud diagram of the structural steel bar under three working conditions. The end near the failed isolation bearing was the near beam end, and the side far from the failed isolation bearing was the far beam end. In the A1 working model, due to the failure of the middle isolation bearing, the upper reinforcement at the far end of the failed isolation bearing beam was broken, and the lower reinforcement near the beam end was broken. The stress distribution was symmetrical with the mid-span symmetry axis. At this time, the compression reinforcement in the beam was under tension. With the gradual shrinkage and failure of the compression reinforcement, the vertical deformation of the remaining structure was divergent and reached the collapse state. In the A2 working model, the steel bar fracture mainly occurred at the far end of the beam, while the steel bar stress of the other side span beam was the smallest. The reason for the analysis was that the lack of sufficient lateral restraint led to a reduction in the remaining structural capacity. In the A3 working model, the damage of the reinforcement at the beam end was similar to that of the middle isolation bearing, and the stress of the reinforcement at the side column increased.

Beam height analyses of the seismic isolation layer

The most significant difference between the base-isolated structure and the ordinary structure was that the seismic isolation layer was added, so the different structural measures of the seismic isolation layer would inevitably lead to the difference in the progressive collapse resistance of the structure. Under normal circumstances, a

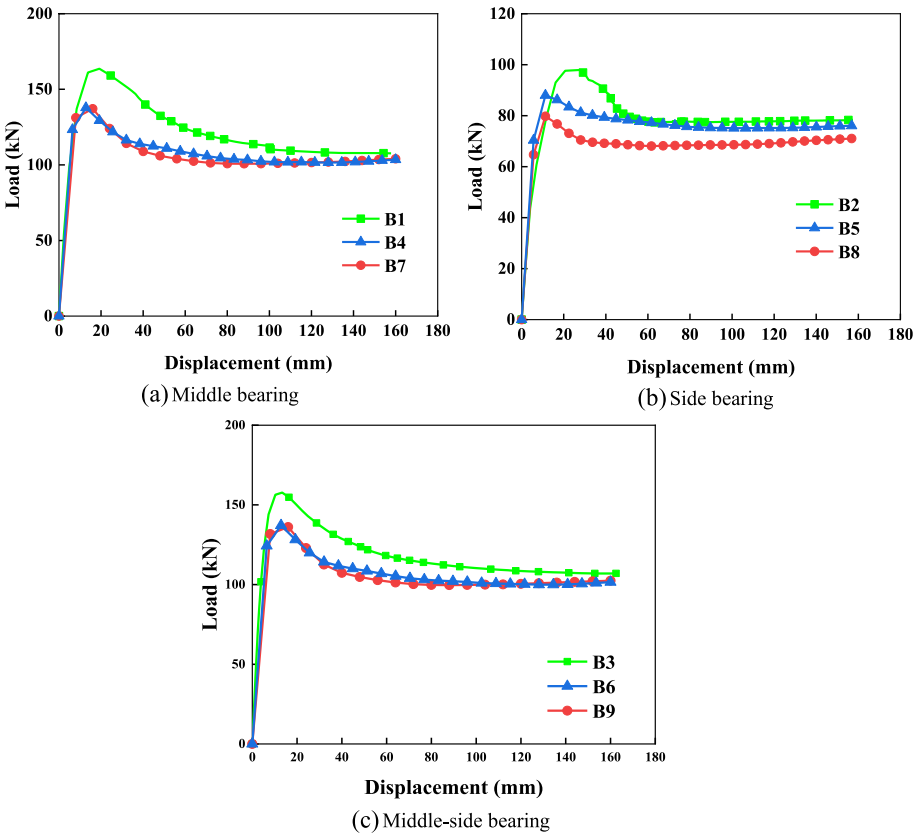

Fig. 19 Load-displacement curves with different beam height**. a** Middle bearing. **b** Side bearing. **c** Middle-side bearing

beam-slab floor would be set on top of the seismic isolation layer, and the relevant parts of the seismic isolation bearing should adopt a cast-in-place concrete beam-slab structure. The capacity of the remaining structure should be greater than general floor slab beams' stiffness and isolation bearing capacity [32]. The requirements in the above code were mainly based on the response characteristics of the structure under earthquake action. The influence of the structural measures of the seismic isolation layer on the progressive collapse resistance of the structure needed to be further studied. Therefore, the failure condition of the seismic isolation bearing was used as the background to compare and analyze the structure progressive collapse resistance performance of the beam of seismic isolation layer of different sizes and then determined its variation law.

When changing the beam size of the seismic isolation layer, the contribution of the seismic isolation floor slab was not considered. That is, the thickness of the seismic isolation floor slab was assumed to be 0mm. The B1-B9 working model was selected for analysis. The capacity of the remaining structure performance of different beam sizes under different working conditions was presented in Fig. 19, and the remaining structural capacity and displacement were illustrated in Table 4. It could be seen from the data in the table that when the beam size of the isolation layer changed, the isolation bearing displacement of the isolation bearing hardly changed. Under the

Table 4 Summary of the capacity of the remaining structure considering the change of beam size in the isolation layer

Working model	Beam mechanism peak (kN)	Beam mechanism displacement (mm)	Catenary peak (kN)	Catenary displacement (mm)	Bearing displacement	
					U_{min}	U_{max}
B1	163.6	20	109.3	142	−22	22
B2	99.7	23	-	-	-	5
B3	157.7	18	112.4	150	−23	21
B4	137.8	18	106.3	147	−20	20
B5	87.9	18	-.	-	-	4
B6	137.1	18	110.4	156	−22	20
B7	136.4	20	109.3	148	−20	20
B8	79.8	17	-	-	-	4
B9	136.1	18	110.2	156	−22	21

condition of different failure positions, the height of the beam of the isolation layer was 175mm and 150mm, respectively, and the peak capacity of the remaining structure was not much different. When the number of isolation layer beams increased, compared with different failure location conditions, the peak isolation bearing capacity of the remaining structures of working model B1 was increased by 18%, 13%, and 15%, respectively, compared with B4, B2, B5, B3, and B9. Therefore, increasing the size of the beam of the isolation layer could improve the remaining structure's isolation capacity, and the beam mechanism's peak value was also slightly increased. Therefore, for a seismic-isolated structure with progressive collapse resistance collapse requirements, the size of the seismic isolation layer's beam should be appropriately increased to improve the capacity of alternate load paths in the remaining structure on the premise of ensuring the essential seismic resistance and structural requirements of the beam of the seismic isolation layer.

Influence of isolation layer isolation bearing type and restraint stiffness

The base-isolated structure differed from the traditional seismic structure, and the different seismic isolation layers of the base-isolated structure had a particular influence on the capacity of the remaining structure against progressive collapse. In establishing a working model, as indicated in Table 2 for comparative analysis, the effects of different isolation bearing types and horizontal restraint stiffness of the seismic isolation layer on the progressive collapse mechanism were studied. Figure 20 was a comparison diagram of pushdown curves under various working conditions. It was found that the peak value of the beam mechanism of the capacity of the remaining structure of the non-base-isolated structure (constrained with 6 degrees of freedom) was slightly higher than the capacity of the remaining structure of the base-isolated structure under the action of the beam mechanism because of the isolation. A summary of the remaining structure's capacity considering the isolation layer's stiffness and the type of isolation bearings is illustrated in Table 5. The change of seismic isolation bearing would not improve the flexural capacity of the beam end of the frame. The horizontal restraint of the seismic

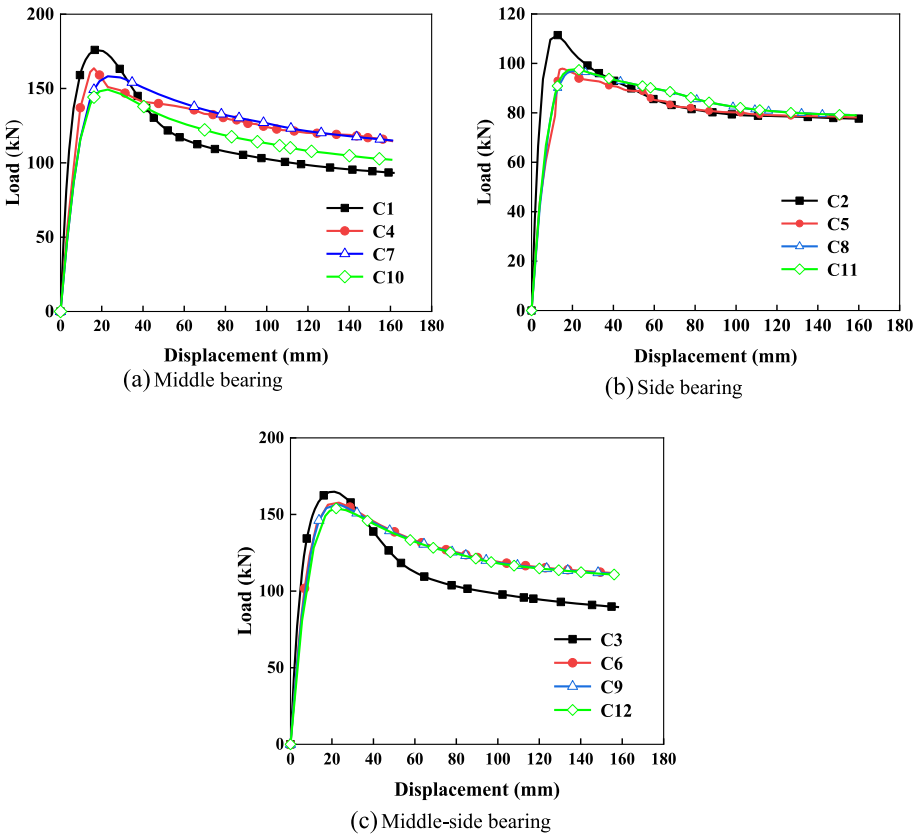

Fig. 20 Load-displacement curves with different types of isolation bearings. a Middle bearing. b Side bearing. c Middle-side bearing

Table 5 Summary of the capacity of the remaining structure considering the stiffness of the isolation layer and the type of isolation bearings

Working model	Beam mechanism peak (kN)	Beam mechanism displacement (mm)	Catenary peak (kN)	Catenary displacement (mm)	Bearing displacement	
					U_{min}	U_{max}
C1	175.9	20	-	-	-	-
C2	11.4	23	-	-	-	-
C3	164.8	18	-	-	-	-
C4	163.6	20	109.3	142	−22	22
C5	99.7	23	-	-	-	5
C6	157.7	18	112.4	150	−23	21
C7	158.23	20	109.2	142	−20	20
C8	96.9	17	-	-	-	4
C9	136.1	18	110.2	150	−22	21
C10	136.4	20	109.3	-	−23	−23
C11	97.6	17	-	-	-	4
C12	156.5	19	109.1	149	−22	21

isolation layer of the base-isolated structure was weaker than that of the non-isolated structure, so the peak capacity of the base-isolated structure was more minor.

At the same time, the existence of the isolation bearing enabled a particular translation and rotation of the beam end of the isolation layer. Therefore, under the condition of removing the short-side middle isolation bearing and inner isolation bearing, the failure of the plastic hinge at the beam end of the base-isolated structure was less than that of the non-base-isolated structure. Seismic structures were delayed. However, base-isolated structure with different isolation bearings and isolation bearings with reduced stiffness has little difference in the vertical collapse capacity of the beam mechanism stage under different failure isolation bearing conditions. In the catenary mechanism stage, the intermediate isolation bearing fails. The capacity of the remaining structure of the base-isolated structure was higher than that of the non-isolated structure under the failure of middle isolation bearing. The reason was that compared with the non-isolated structure, the damage of the plastic hinge at the beam end of the base-isolated structure was delayed, so the deformation of the catenary mechanism was also delayed, resulting in the capacity of the remaining structure decrease. Due to the lack of sufficient lateral restraint, the vertical capacity of the non-base-isolated structure and the base-isolated structure in the catenary stage were not much different in the case of side isolation bearing failure.

Limited by the test conditions, the test model in this study is a two-dimensional plane model, which cannot fully reflect the progressive collapse mechanism of the actual three-dimensional model. Therefore, the progressive collapse resistance of the actual base-isolated structure should be much stronger. However, since the isolation layer is far less constrained than other floors, the isolation structure cannot form an effective beam mechanism and catenary mechanism like the non-isolation structure to give full play to the progressive collapse resistance of the remaining structure. Therefore, it is very necessary to carry out a special anti-progressive collapse design for the seismic isolation structure with a high risk of extreme events.

Conclusions

From the results of the current study, the following conclusions can be drawn:

(1) Releasing the reaction force from the seismic isolation layer could protect the adjacent internal members to a certain extent. As the vertical displacement of the center column increases, the stress on both sides of the adjacent isolation bearings of the failed isolation bearing would intensify the compressive stress distribution. The non-uniformity of the beams and the concentrated loading at the nodes was easy to form a linear catenary mechanism, resulting in more severe beam end damage than mid-span damage.

(2) In the case of side isolation bearing failure, due to the lack of sufficient lateral restraint, the capacity was significantly lower than other conditions, which were more likely to cause partly collapse. Therefore, setting more transfer paths for the base-isolated structure was necessary to strengthen the progressive collapse resistance of structures.

(3) Increasing the size of the beam of the seismic isolation layer could improve the capacity of the remaining structure of the alternate load path in the base-isolated structure. For the base-isolated structure which needs to resist progressive collapse, the size of the beam of the seismic isolation layer could be appropriately increased to improve

the capacity of the remaining structure of the alternate load path in a base-isolated structure.

(4) Due to the weakening of the isolation layer's restraint, the isolation bearing allows a particular translation and rotation of the beam end of the seismic isolation layer, and the base-isolated structure reaches the peak value of the beam mechanism under the condition of removing the inner isolation bearing. The changes in the horizontal stiffness of the seismic isolation layer and the type of the isolation bearing have little effect on the progressive collapse resistance capacity of the remaining structure.

Abbreviations

RC	Reinforced concrete
LRB	Lead rubber bearing
f_y	Yield strength of reinforcing
f_t	Ultimate strength of reinforcement
ε_{max}	Maximum principal strain
δ	The vertical displacement of the top of the failed column
Δ	The horizontal displacement of the bearing

Acknowledgements
Not applicable.

Authors' contributions
The corresponding author, Assoc. Prof. Dr. Bao: ideas, development, and design of methodology and writing-original draft preparation. Zhang: data curation, writing, and editing. Lv: formal analysis software and mathematical analysis. Wang: visualization and investigation. Ma: writing-reviewing and editing. Cao and Lim: supervision. The authors read and approved the final manuscript.

Funding
This research was funded by the Natural Science Foundation of Ningxia 2022AAC03266, Ningxia Key Research and Development Program grant number 2021BEG03022, Ningxia Key Research and Development Program (Special Talents) grant number 2018BEB04006, "West Light" Foundation of The Chinese Academy of Sciences grant number XAB2021YW14, and Ningxia Outstanding Talent Support Program Project grant number TJGC2019001 and TJGC2019007.

Availability of data and materials
All data generated or analyzed during this study are included in this published article.

Declarations

Ethics approval and consent to participate
Not applicable.

Consent for publication
Not applicable.

Competing interests
The authors declare that they have no competing interests.

Received: 18 August 2022 Accepted: 31 October 2022
Published online: 12 December 2022

References

1. Pearson C, Delatte N (2005) Ronan Point apartment tower collapse and its effect on building codes. J Perform Constr Fac 19(2):172–177. https://doi.org/10.1061/(asce)0887-3828(2005)19:2(172)
2. Osteraas JD (2006) Murrah building bombing revisited: a qualitative assessment of blast damage and collapse patterns. J Perform Constr Fac 20(4):330–335. https://doi.org/10.1061/(asce)0887-3828(2006)20:4(330)
3. Bažant ZP, Zhou Y (2002) Why did the world trade center collapse?—simple analysis. J Eng Mech 128(1):2–6. https://doi.org/10.1061/(asce)0733-9399(2002)128:1(2)
4. Ren PQ, Li Y, Lu XZ et al (2016) Experimental investigation of progressive collapse resistance of one-way reinforced concrete beam–slab substructures under a middle-column-removal scenario. Eng Struct 118:28–40. https://doi.org/10.1016/j.engstruct.2016.03.051
5. Adam JM, Parisi F, Sagaseta J et al (2018) Research and practice on progressive collapse and robustness of building structures in the 21st century. Eng Struct 173:122–149. https://doi.org/10.1016/j.engstruct.2018.06.082

6. Liu Y, Yan J, Li Z et al (2019) Improved SDOF and numerical approach to study the dynamic response of reinforced concrete columns subjected to close-in blast loading. Structures 22:341–365. https://doi.org/10.1016/j.istruc.2019.08.014
7. Qiu L, Lin F, Wu K (2020) Improving progressive collapse resistance of RC beam-column subassemblages using external steel cables. J Perform Constr Fac 34(1):04019079. https://doi.org/10.1061/(asce)cf.1943-5509.0001360
8. Kunnath SK, Bao Y, El-Tawil S (2018) Advances in computational simulation of gravity-induced disproportionate collapse of RC frame buildings. J Struct Eng 144(2):03117003. https://doi.org/10.1061/(asce)st.1943-541x.0001938
9. Yu J, Gan YP, Wu J et al (2019) Effect of concrete masonry infill walls on progressive collapse performance of reinforced concrete infilled framework. Eng Struct 191:179–193. https://doi.org/10.1016/j.engstruct.2019.04.048
10. Qiang H, Yang J, Feng P et al (2020) Kinked rebar configurations for improving the progressive collapse behaviours of RC framework under middle column removal scenarios. Eng Struct 211:110425. https://doi.org/10.1016/j.engstruct.2020.110425
11. Lu XZ, Lin KQ, Li CF et al (2018) New analytical calculation models for compressive arch action in reinforced concrete structures. Eng Struct 168:721–735. https://doi.org/10.1016/j.engstruct.2018.04.097
12. Xiao YZ, Li Y, Lu XZ et al (2019) Experimental study on the dynamic effects in progressive collapse of beam-column concrete substructures. Eng Mech 36(5):44–52.(in Chinese). https://doi.org/10.6052/j.issn.1000-4750.2018.04.0189
13. Qian K, Lan DQ, Fu F et al (2020) Effects of infilled wall opening load resisting capacity of RC framework to mitigate progressive collapse risk. Eng Struct 223:111196. https://doi.org/10.1016/j.engstruct.2020.111196
14. Amiri S, Saffari H, Mashhadi J (2018) Assessment of dynamic increase factor for progressive collapse analysis of RC structures. Eng Fail Anal 84:300–310. https://doi.org/10.1016/j.engfailanal.2017.11.011
15. Jiang LQ, Ye JH, Zheng H (2019) Collapse mechanism analysis of the FIU pedestrian bridge based on the improved structural vulnerability theory (ISVT). Eng Fail Anal 104:1064–1075. https://doi.org/10.1016/j.engfailanal.2019.06.033
16. Azim I, Yang J, Bhatta S et al (2020) Factors influencing the progressive collapse resistance of RC frame structures. J Build Eng 27:100986. https://doi.org/10.1016/j.jobe.2019.100986
17. Feng DC, Xie SC, Li Y et al (2021) Time-dependent reliability-based redundancy assessment of deteriorated RC structures against progressive collapse considering corrosion effect. Struct Saf 89:102061. https://doi.org/10.1016/j.strusafe.2020.102061
18. Lu XZ, Lin KQ, Li Y et al (2017) Experimental investigation of RC beam-slab substructures against progressive collapse subject to an edge-column-removal scenario. Eng Struct 149:91–103. https://doi.org/10.1016/j.engstruct.2016.07.039
19. Yu J, Luo LZ, Fang Q (2020) Structure behavior of reinforced concrete beam-slab assemblies subjected to perimeter middle column removal scenario. Eng Struct 208:110336. https://doi.org/10.1016/j.engstruct.2020.110336
20. Ma FH, Gilbert BP, Guan H et al (2019) Experimental study on the progressive collapse behaviour of RC flat plate substructures subjected to corner column removal scenarios. Eng Struct 180:728–741. https://doi.org/10.1016/j.engstruct.2018.11.043
21. Kai Q, Liang SL, Feng DC et al (2020) Experimental and numerical investigation on progressive collapse resistance of post-tensioned precast concrete beam-column sub-assemblages. J Struct Eng 146(9):04020170. https://doi.org/10.1061/(asce)st.1943-541x.0002714
22. Deng XF, Liang SL, Fu F et al (2020) Effects of high strength concrete on progressive collapse resistance of reinforced concrete frame. J Struct Eng 146(6):04020078. https://doi.org/10.1061/(asce)st.1943-541x.0002628
23. Wang Y, Zhang B, Gu XL et al (2022) Experimental and numerical investigation on progressive collapse resistance of RC frame structures considering transverse beam and slab effects. J Build Eng 47:103908. https://doi.org/10.1016/j.jobe.2021.103908
24. Liu YL, Zhao ZD, Cheng XW et al (2022) Experimental and numerical investigation of the progressive collapse of precast reinforced concrete frame substructures with wet connections. Eng Struct 256:114010. https://doi.org/10.1016/j.engstruct.2022.114010
25. Tavakoli HR, Naghavi F, Goltabar AR (2015) Effect of base isolation systems on increasing the resistance of structures subjected to progressive collapse. Earthq Struct 9(3):639–656 https://doi.org/10.12989/eas.2015.9.3.639
26. Huang XN, Wang N, Du YF (2019) Reliability analysis of the vertical progressive collapse of base-isolated frame-wall structures under earthquakes. Eng Mech 36(9):89-94,127. https://doi.org/10.6052/j.issn.1000-4750.2018.07.0389
27. Yang Y, Chen A, Yang T (2019) Progressive collapse of the base-isolated frame structures supported by stepped foundation in mountainous city. Applied Sciences 12(4):2151. https://doi.org/10.3390/app12042151
28. Khandelwal K, El-Tawil S (2008) Assessment of progressive collapse residual capacity using pushdown analysis. In Structures Congress 2008: Crossing Borders pp: 1-8. https://doi.org/10.1061/41016(314)94
29. Ministry of Housing and Urban-Rural Development of the People's Republic of China (2021) GB/T 51408-2021. Standard for seismic isolation design of building, China
30. United States General Services Administration (2016) Progressive collapse analysis and design guidelines for new federal office buildings and major modernization projects. USA, Washington DC
31. Department of Defense (2016) Design of buildings to resist progressive collapse unified facilities criteria (UFC): 4-023-16, Washington DC
32. Ministry of Housing and Urban-Rural Development of the People's Republic of China (2010) GB 50010-2010. Code for Design of Concrete Structures, China

Publisher's Note